Composite Structures 108 (2014) 456–471

Contents lists available at ScienceDirect

Composite Structures

journal homepage: www.elsevier.com/locate/compstruct

Delamination in laminated plates using the 4-noded quadrilateral QLRZ plate element based on the refined zigzag theory

A. Eijo *, E. Oñate, S. Oller

International Center for Numerical Methods in Engineering (CIMNE), Universitat Politècnica de Catalunya (UPC), Campus Norte UPC, 08034 Barcelona, Spain

ARTICLE INFO

Article history:
Available online 3 October 2013

Keywords:
Laminated plates
Delamination
QLRZ plate element

ABSTRACT

A numerical method based on the Refined Zigzag Theory (RZT) to model delamination in composite laminated plate/shell structures is presented. The originality of this method is the use of 4-noded quadrilateral plate finite elements whit only seven variables per node to discretize the plate/shell geometry. The ability to capture the relative displacement between consecutive layers in fracture mode II and III is the more important advantage of this element, denoted QLRZ [1].

A continuum isotropic damage model [2] is used to model the mechanical behavior of the plies. The material non-lineal problem is solved with the modified Newton–Raphson method.

The RZT plate theory, the QLRZ finite element and the isotropic damage model are described in this work. Also, the implicit integration algorithm is presented. The performance of the numerical model is analyzed by studying the delamination in a rectangular plate for two different laminates, using the 3D analysis as the reference solution.

1. Introduction

Delamination [3] is a dangerous failure mode in laminated composite materials and is normally characterized by a relative displacement between layers due to a loss of adherence. Local forces, thermal actions and low energy impacts may serve as sources of delamination during the transportation, storage or service life of the structural member. In addition, geometry discontinuities such as access holes, notches, free edges or bonded and bolted joints can also induce delamination due to high stress gradients. Once delamination has occurred, the initial stiffness of the structure could be considerably reduced which can induce the structural failure by other phenomena as buckling, excessive vibration or fatigue.

During the design phases of laminated structures, it is important to know how the global response of the structure will be affected by delamination. Thus, much effort and time is been invested to develop numerical tools that can predict delamination in an effective and efficient manner.

The more common procedures to model delamination are based on the fracture mechanics or the damage mechanics. The virtual crack closure technique (VCCT) [4–6] and the cohesive finite elements [7–11] are some typical examples. Each of these techniques has their own drawbacks, but they share one of the most inefficient features: the need to place interface fracture or cohesive finite elements between the plies where delamination is expected to occur. Because of the delamination path is normally unknown, it is necessary to place interface elements between all layers, which leads to an increase of computational resources needed to carry out the simulation, specially in laminates with many plies. In order to avoid the above-mentioned disadvantage, Martinez et al. [12] have studied delamination under the continuum mechanics using a 3D finite element method and an isotropic damage model to manage material degradation.

The capabilities of 3D models are well known. However, the computational resources needed for modeling non-linear problems grow significantly when 3D finite elements are used to discretize the structure. Although there are several cases where a 3D analysis is indispensable, for instance for studying the delamination in bonded joints, it is almost computationally impossible to use them for large laminated composite structures with tens of layers such as wind turbine blades or aircraft fuselage. For these kinds of structures, more simplified models should be used.

Some examples of simple models used to simulate laminated composite plate/shell structures are the First Order Shear Deformation Theory (FSDT) [13,14], the Layer-Wise theories (LWT) [15–18], the ZigZag (ZZ) theories [17,19–21] and the *Refined ZigZag Theory* (RZT) [22–26].

Despite the simplicity of the FSDT theory, it is well documented [1,27] that this model gives wrong predictions for highly heterogeneous laminates. In addition, the FSDT is unable to capture delamination because of its linear kinematics assumptions.

* Corresponding author. Tel.: +34 934010808.
E-mail address: aeijo@cimne.upc.edu (A. Eijo).

0263-8223/$ - see front matter © 2013 Elsevier Ltd. All rights reserved.
http://dx.doi.org/10.1016/j.compstruct.2013.09.052

LWT models describe separately the displacement field within each ply, which leads to a high level of refinement of the kinematics. Because of that, they can reproduce with high precision the complex kinematics of highly heterogeneous laminates, and also simulate the delamination phenomenon [28,29]. However, since the number of unknowns is proportional to the number of analysis sublayers (that may be not coincident with the number of physical layers), the computational cost increases with the number of subdivisions.

ZZ theories are an attractive compromise between the high accuracy of LWT and the computational efficiency of FSDT. The kinematics is defined as a superposition of a piecewise linear displacement functions over a linear, quadratic or cubic displacement field along the thickness direction. The number of kinematics variables is independent of the number of layers, which favors the efficiency. Despite its good performance, they present some difficulties to model correctly some boundary condition. So far, the use of the ZZ theories to model delamination in beams and plates has been quite limited. A ZZ model to simulate delamination has been developed by Icardi and Zardo [30].

The kinematics proposed by the RZT theory is defined by a superposition of a linear piecewise zigzag function over the FSDT displacement fields. Since RZT is an improvement of the ZZ theories, the number of variables is also independent of the number of plies. However, unlike the ZZ, all boundary conditions, including the fully clamped condition, can be simulated effectively as it was demonstrated in the original paper [23,24]. Oñate et al. [25,27] and Eijo et al. [1] have taken the RZT as the basis for developing linear beam (LRZ) and quadrilateral plate (QLRZ) finite elements, respectively.

Eijo et al. [31] have extended the LRZ element to simulate delamination in laminated beams. Since the vertical displacement is defined constant along the thickness and the transversal in-plane displacement is not considered for the RZT beam theory, the proposed methodology is limited to model only the fracture mode II. In addition, delamination in highly heterogeneous laminates, i.e. laminates where the shear modulus of the laminae differ from each other in many orders of magnitude can not be correctly simulated employing this technique. However, that is not the case of composite laminates where the shear modulus of laminae does not differ generally in more than one order of magnitude [32]. For this model, delamination can happen at any place within the laminate, thus, it is not necessary to predefine the path where crack is expected to occur. An isotropic damage model was used to manage the non-linear material behavior. It was demonstrated that, in order to be able for capturing relative displacements between layers, the piecewise zigzag function must be updated in terms of the damage level of the material. In [31] it was shown not only the ability to capture the relative displacement between layers, but also the efficiency of the numerical model based on the RZT theory.

In this paper, we present the extension of the beam delamination model of [31] to plate/shell structures using the QLRZ element. Unlike the beam theory, the transversal in-plane displacement is taken into account for the plate theory, which allows simulating not only the fracture mode II but also mode III. For the same reason as in beams, it is not possible to predict the opening fracture mode. The non-linear material behavior is modeled using an isotropic damage model. The non-linear problem is solved by the modified Newton–Raphson method. The paper describes the RZT plate theory, the formulation of the QLRZ finite elements and the isotropic damage model. Also, the implicit integration algorithm is described. Finally, the performance of the proposed numerical model is shown by modeling delamination in a simply supported rectangular plate with a center hole for two different laminates. The reference solution is a 3D analysis using eight-noded hexahedral elements.

2. Refined Zigzag Theory (RZT) for plate and QLRZ plate/shell element

2.1. RZT plate kinematics

A laminated plate formed by N analysis layers of thickness h^k is considered. The number of analysis layer may be not coincident with the number of physical layers. The reference coordinate system is the 3D Cartesian system (x,y,z), where x–y are set as the in-plane coordinates and z is the thickness coordinate.

The plate displacement field proposed by the RZT is defined as (Fig. 1)

$$\begin{aligned} u^k(x,y,z) &= u_0(x,y) - z\cdot\theta_x(x,y) + \bar{u}^k(x,y,z)\\ v^k(x,y,z) &= v_0(x,y) - z\cdot\theta_y(x,y) + \bar{v}^k(x,y,z)\\ w(x,y) &= w_0(x,y) \end{aligned} \tag{1a}$$

where the linear piecewise zigzag functions are

$$\begin{aligned} \bar{u}^k &= \phi_x^k(z)\cdot\psi_x(x,y); \quad k=1,N\\ \bar{v}^k &= \phi_y^k(z)\cdot\psi_y(x,y) \end{aligned} \tag{1b}$$

and superscript k indicates quantities within the kth layer with $z_k \leqslant z \leqslant z_{k+1}$, and z_k is the vertical coordinate of the kth interface. The *uniform axial displacements* along the coordinate directions x and y are u_0 and v_0, respectively; θ_x and θ_y represent the *average bending rotation* of the transverse normal about the negative y and positive x directions; and w_0 is the *transverse deflection*.

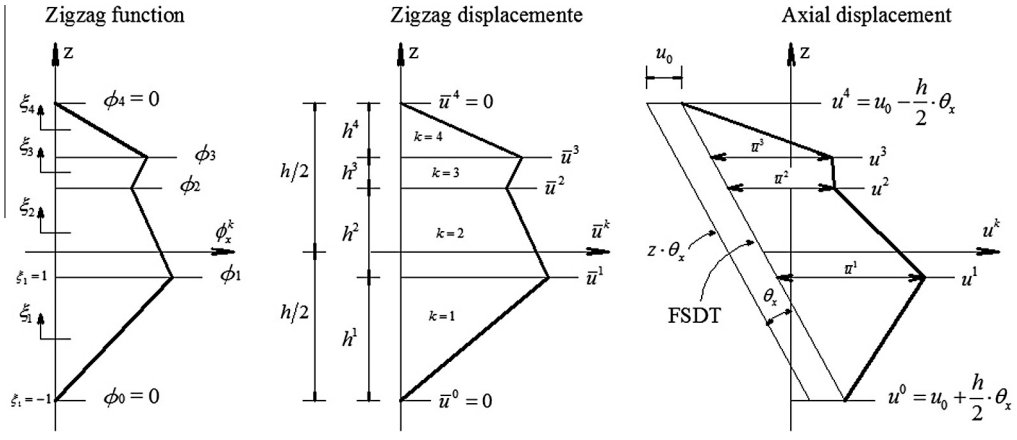

Fig. 1. RZT kinematics.

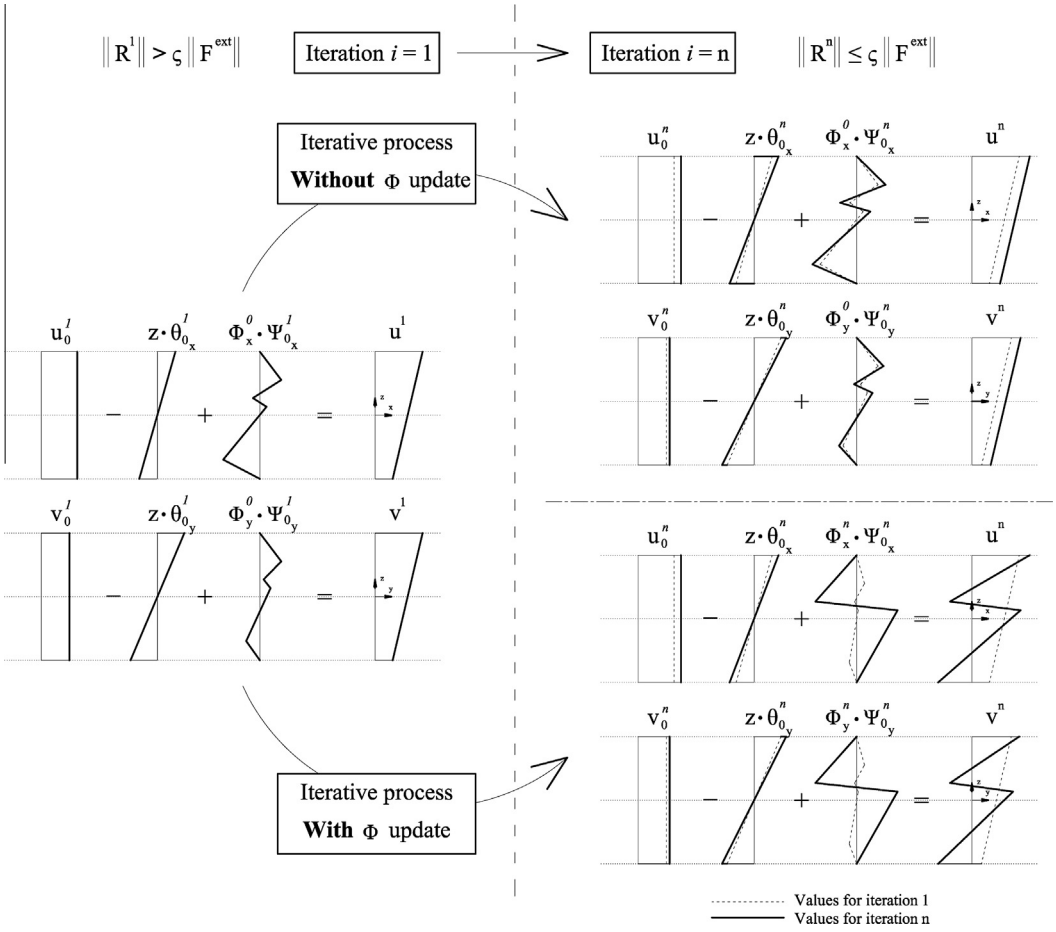

Fig. 2. Iterative process with and without update of ϕ_i ($i = x,y$). Delamination can be captured using the QLRZ finite element when the zigzag function ϕ_i is updated by reducing the shear modulus of the damaged layer.

$\phi_i^k(i = x, y)$ denotes a known piecewise linear *zigzag function*, and ψ_i is a primary kinematic variable defining the *amplitude of the zigzag function* on the plate.

Summarizing, the kinematic variables are

$$\mathbf{a} = \begin{bmatrix} u_0 & v_0 & w_0 & \theta_x & \theta_y & \psi_x & \psi_y \end{bmatrix}^T \tag{2}$$

The in-plane $\boldsymbol{\varepsilon}_p^k$ and the transverse shear $\boldsymbol{\varepsilon}_t^k$ strains are defined as

$$\boldsymbol{\varepsilon}^k = \begin{bmatrix} \boldsymbol{\varepsilon}_p \\ \boldsymbol{\varepsilon}_t \end{bmatrix}^k = \begin{bmatrix} \varepsilon_x \\ \varepsilon_y \\ \gamma_{xy} \\ \gamma_{xz} \\ \gamma_{yz} \end{bmatrix}^k = \begin{bmatrix} \frac{\partial u^k}{\partial x} \\ \frac{\partial v^k}{\partial y} \\ \frac{\partial u^k}{\partial y} + \frac{\partial v^k}{\partial x} \\ \frac{\partial u^k}{\partial z} + \frac{\partial w}{\partial x} \\ \frac{\partial v^k}{\partial z} + \frac{\partial w}{\partial y} \end{bmatrix}$$

$$= \begin{bmatrix} \frac{\partial u_0}{\partial x} \\ \frac{\partial v_0}{\partial y} \\ \frac{\partial u_0}{\partial y} + \frac{\partial v_0}{\partial x} \\ 0 \\ 0 \end{bmatrix} + \begin{bmatrix} -z\frac{\partial \theta_x}{\partial x} \\ -z\frac{\partial \theta_y}{\partial y} \\ -z\left(\frac{\partial \theta_x}{\partial y} + \frac{\partial \theta_y}{\partial x}\right) \\ \frac{\partial w_0}{\partial x} - \theta_x \\ \frac{\partial w_0}{\partial y} - \theta_y \end{bmatrix} + \begin{bmatrix} \phi_x^k(z)\frac{\partial \psi_x}{\partial x} \\ \phi_y^k(z)\frac{\partial \psi_y}{\partial y} \\ \phi_x^k(z)\frac{\partial \psi_x}{\partial y} + \phi_y^k(z)\frac{\partial \psi_y}{\partial x} \\ \frac{\partial \phi_x^k}{\partial z}\psi_x \\ \frac{\partial \phi_y^k}{\partial z}\psi_y \end{bmatrix} \tag{3}$$

which can be written in matrix form as

$$\boldsymbol{\varepsilon}^k = \begin{bmatrix} \boldsymbol{\varepsilon}_p^k \\ \boldsymbol{\varepsilon}_t^k \end{bmatrix} = \begin{bmatrix} \mathbf{S}_p & \mathbf{0} \\ \mathbf{0} & \mathbf{S}_t \end{bmatrix}^k \cdot \begin{bmatrix} \hat{\boldsymbol{\varepsilon}}_p \\ \hat{\boldsymbol{\varepsilon}}_t \end{bmatrix} = S^k \hat{\boldsymbol{\varepsilon}} \tag{4}$$

where $\hat{\boldsymbol{\varepsilon}}$ is the generalized stain vector.

2.2. Derivation of the zigzag function ϕ

The zigzag function is defined within each layer as

$$\phi_i^k = \bar{\phi}_i^{k-1} + \frac{h^k \beta_i^k}{2}(\zeta^k + 1) \quad i = x, y \tag{5}$$

where $\bar{\phi}_i^k$ and $\bar{\phi}_i^{k-1}$ are the zigzag function valued at k and $k-1$ interface, respectively with $\bar{\phi}_i^0 = \bar{\phi}_i^N = 0$ and $\zeta^k = 2\frac{(z - z^{k-1})}{h^k} - 1$. The slope $\beta_i^k = \frac{\partial \phi_i^k}{\partial z}$ of the zigzag function within each layer is expressed as

$$\beta_i^k = \frac{G_{iz}}{G_{iz}^k} - 1 \tag{6}$$

where G_{iz} is an average shear modulus that can be expressed in terms of the shear modulus $\left(G_{iz}^k\right)$ and the thickness (h^k) of each layer as

$$G_{iz} = h\left[\sum_{k=1}^{N} \frac{h^k}{G_{iz}^k}\right]^{-1} \tag{7}$$

For a more detailed description of the RZT for plates, the readers are referred to Tessler et al. [23].

2.3. Stresses and resultant stresses

The relationship between the stresses and the strains for the kth layer are expressed in matrix form as

 # Loop over load increments

Update external forces $\mathbf{F}^{\text{ext}}$

 # Iterative process

If *i*th iteration = 1

$${}^{1}\mathbf{a} = \mathbf{K}_{\text{d}}{}^{-1} \cdot \mathbf{F}^{\text{ext}}$$

$${}^{1}\boldsymbol{\varepsilon}^{k} = \mathbf{S}^{k}\ \mathbf{B}\ {}^{1}\mathbf{a}$$

Note that for the first iteration both $\mathbf{K}_{\text{d}}{}^{-1}$ and $\mathbf{S}^{k}$ were computed at the last iteration of the previous load increment.

Else

$${}^{i}d\mathbf{a} = {}^{i-1}\mathbf{K}_{\text{d}} \cdot {}^{i-1}\mathbf{R}$$

$${}^{i}\mathbf{a} = {}^{i-1}\mathbf{a} + {}^{i}d\mathbf{a}$$

$${}^{i}\boldsymbol{\varepsilon}^{k} = {}^{i-1}\mathbf{S}^{k}\ \mathbf{B}\ {}^{i}\mathbf{a}$$

Remember that ${}^{i-1}\mathbf{S}^{k}$ contains ${}^{i-1}\phi_{x}^{k}$, ${}^{i-1}\phi_{y}^{k}$, ${}^{i-1}\tilde{\beta}_{x}^{k}$ and ${}^{i-1}\tilde{\beta}_{y}^{k}$ computed at the previous iteration.

End if

Evaluate undamaged stresses

$${}^{i}\boldsymbol{\sigma}_{0}^{k} = \mathbf{D}_{0}^{k} \cdot {}^{i}\boldsymbol{\varepsilon}^{k}$$

Compute damage variable:

$${}^{i}d^{k} = 1 - \frac{c_0}{{}^{i}f} e^{B\left(1 - \frac{{}^{i}f}{c_0}\right)} \qquad \text{with} \qquad {}^{i}f = \sqrt{{}^{i}\boldsymbol{\varepsilon}^{k} : {}^{i}\boldsymbol{\sigma}_{0}^{k}}$$

Update stresses and shear modulus:

$${}^{i}\boldsymbol{\sigma}^{k} = \left(1 - {}^{i}d^{k}\right){}^{i}\boldsymbol{\sigma}_{0}^{k}$$

$${}^{i}\tilde{G}_{xz}^{k} = \left(1 - {}^{i}d^{k}\right){}^{i}G_{xz0}^{k} \quad ; \quad {}^{i}\tilde{G}_{yz}^{k} = \left(1 - {}^{i}d^{k}\right){}^{i}G_{yz0}^{k}$$

Update zigzag function:

$${}^{i}\tilde{G}_{xz} = h\left[\sum_{k=1}^{N} \frac{h^{k}}{{}^{i}\tilde{G}_{xz}^{k}}\right]^{-1} \quad ; \quad {}^{i}\tilde{G}_{yz} = h\left[\sum_{k=1}^{N} \frac{h^{k}}{{}^{i}\tilde{G}_{yz}^{k}}\right]^{-1}$$

$${}^{i}\tilde{\beta}_{x}^{k} = \frac{{}^{i}\tilde{G}_{xz}}{{}^{i}\tilde{G}_{xz}^{k}} - 1 \quad ; \quad {}^{i}\tilde{\beta}_{y}^{k} = \frac{{}^{i}\tilde{G}_{yz}}{{}^{i}\tilde{G}_{yz}^{k}} - 1$$

$${}^{i}\phi_{x}^{k} = \bar{\phi}_{x}^{k-1} + \frac{h^{k}\,{}^{i}\tilde{\beta}_{x}^{k}}{2}\left(\zeta^{k} + 1\right) \quad ; \quad {}^{i}\phi_{y}^{k} = \bar{\phi}_{y}^{k-1} + \frac{h^{k}\,{}^{i}\tilde{\beta}_{y}^{k}}{2}\left(\zeta^{k} + 1\right)$$

Computation of the secant stiffness matrix and internal forces:

$${}^{i}\mathbf{K}_{\text{d}} = \int_{l} \mathbf{B}^{T}\ {}^{i}\hat{\mathbf{D}}_{\text{d}}\ \mathbf{B}\ dl$$

$${}^{i}\mathbf{F}^{\text{int}} = \int_{V} \mathbf{B}^{T}\ {}^{i}\mathbf{S}^{T}\ {}^{i}\boldsymbol{\sigma}^{k}\, dV$$

Verification of convergence criteria

$$\mathbf{F}^{\text{ext}} - {}^{i}\mathbf{F}^{\text{int}} = {}^{i}\mathbf{R}$$

$$\left\| {}^{i}\mathbf{R} \right\| \leq \varsigma \left\| \mathbf{F}^{\text{ext}} \right\|$$

 # END iterative process

 # END loops over load increments

Fig. 3. Algorithm for solving the non-linear problem using the modified Newton–Raphson method. Note that the zigzag function is updated at each iteration.

$$\boldsymbol{\sigma}^{k} = \begin{bmatrix} \boldsymbol{\sigma}_{p} \\ \boldsymbol{\sigma}_{t} \end{bmatrix}^{k} = \begin{bmatrix} \sigma_{x} \\ \sigma_{y} \\ \tau_{xy} \\ \tau_{xz} \\ \tau_{yz} \end{bmatrix}^{k} = \begin{bmatrix} \mathbf{D}_{p} & \mathbf{0} \\ \mathbf{0} & \mathbf{D}_{t} \end{bmatrix}^{k} \cdot \begin{bmatrix} \boldsymbol{\varepsilon}_{p} \\ \boldsymbol{\varepsilon}_{t} \end{bmatrix}^{k} = \mathbf{D}^{k}\boldsymbol{\varepsilon}^{k} \tag{8}$$

with

$$\mathbf{D}_{p}^{k} = \frac{1}{1 - \upsilon_{xy}\upsilon_{yx}} \begin{bmatrix} E_{x} & \upsilon_{xy}E_{x} & 0 \\ \upsilon_{yx}E_{x} & E_{y} & 0 \\ 0 & 0 & (1 - \upsilon_{xy}\upsilon_{yx})G_{xy} \end{bmatrix} \tag{9}$$

$$\mathbf{D}_{t}^{k} = \begin{bmatrix} G_{xz} & 0 \\ 0 & G_{yz} \end{bmatrix}$$

where E, G, υ and $\mathbf{D}$ are the Young modulus, the shear modulus, the Poisson's ratio and the constitutive matrix for the kth layer, respectively.

The stress resultants are computed by integrating the stresses over the plate thickness as

$$\hat{\boldsymbol{\sigma}} = \int_{z} \mathbf{S}^{k}\boldsymbol{\sigma}^{k}\, dz \tag{10}$$

2.4. QLRZ plate/shell element

The middle surface of the plate is discretized using quadrilateral 4-noded C^0 finite elements. Thus, the kinematics variables of Eq. (2) are interpolated within each element e as

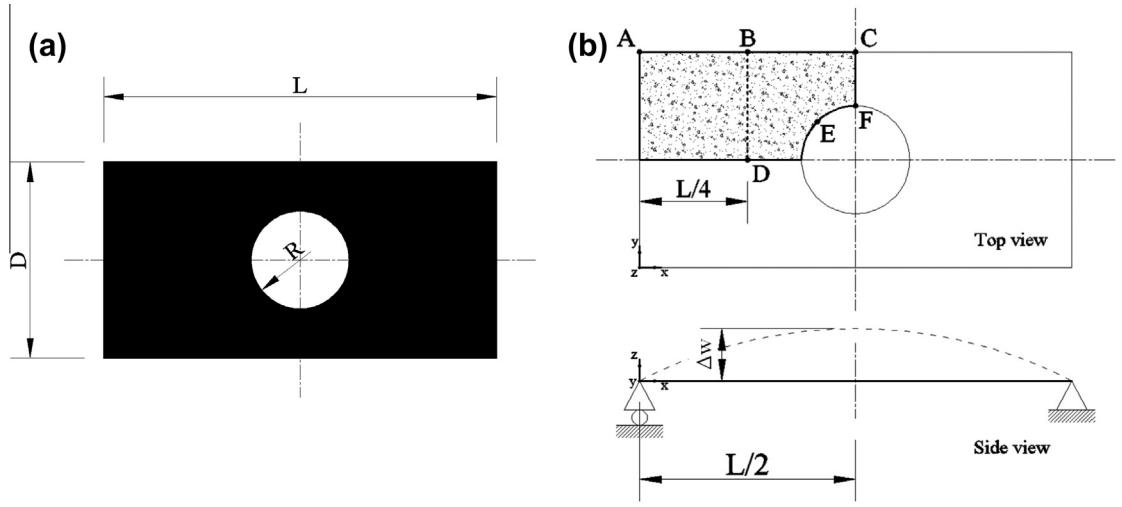

Fig. 4. Simply supported rectangular plate with a center hole. Whole structure dimensions (a), quarter of plate under study with boundary conditions (b).

Table 1
Mechanical properties of linear-elastic layers.

Materials	Young's modulus			Shear modulus			Poisson
	E_x	E_y	E_z	G_{xy}	G_{xz}	G_{yz}	μ
Mechanical properties of linear-elastic plies (MPa)							
A	157.9×10^4	9.584×10^4	9.584×10^4	5.93×10^4	5.93×10^4	3.227×10^4	0.32
B	19.15×10^2	19.15×10^2	19.15×10^3	42.3×10^{-5}	36.51×10^2	124.8×10^2	6.58×10^{-4}
C		104.0×10^1			4.00×10^2		0.30
D		5.30×10^1			2.12×10^1		0.25
E		2.19×10^1			0.876×10^1		0.25
F		0.82×10^1			0.328×10^1		0.25
G		0.73×10^{-1}			0.29×10^{-1}		0.25
H		7.3×10^1			2.92×10^1		0.25

Table 2
Mechanical properties of cohesive layers (cl).

Materials	Young's modulus (E_0) (MPa)	Shear modulus (G_0) (MPa)	Tensile strength (f_t) (MPa)	Fracture energy (G_f) (kN/m)
Mechanical properties of cohesive plies (cl)				
I^{cl}	104.0×10^1	4.0×10^2	2.0×10^1	5.0×10^4
J^{cl}	0.73×10^{-1}	0.29×10^{-1}	3.0×10^{-4}	5.0×10^4

Table 3
Layer distribution of laminated materials.

Laminate	Layer distribution	h^k/h	h (mm)
Laminated materials			
L1	(A/C/A/C/B/I^{cl}/C/A/C/A)	(1.0/0.12/0.1/0.08/0.14/0.02/0.08/0.1/0.06/0.2)	25.0
L2	(D/E/F/G/D/J^{cl}/H/F/E/H)	(1.0/0.12/0.1/0.08/0.14/0.02/0.08/0.1/0.06/0.2)	25.0

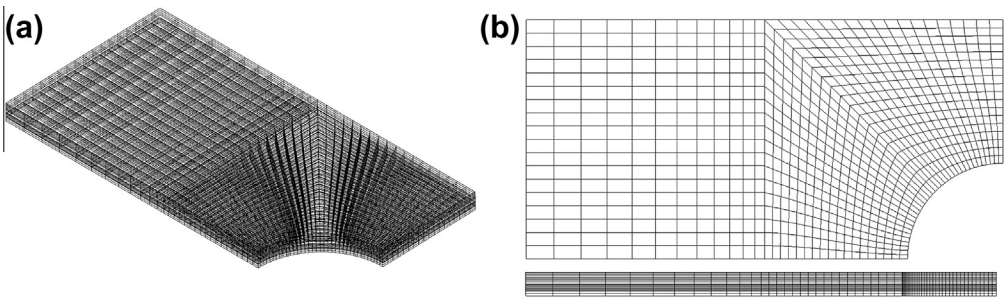

Fig. 5. HEXA8 mesh for both laminates. Isometric view (a), top and side view (b).

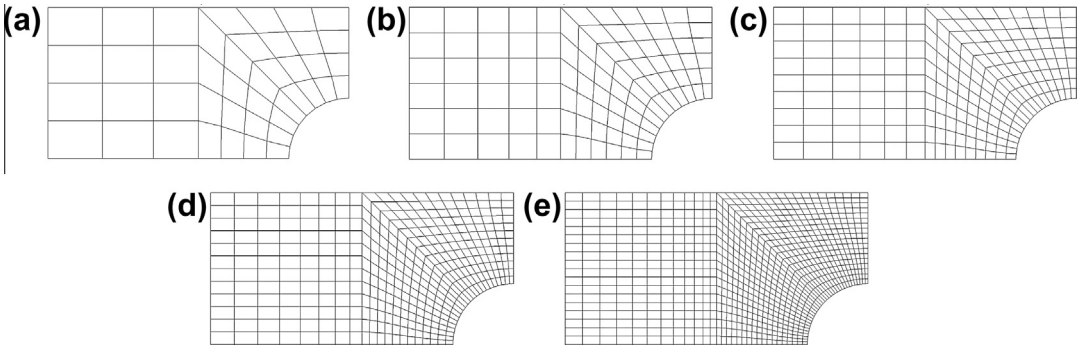

Fig. 6. QLRZ meshes of 44 (a), 102 (b), 216 (c), 384 (d) and 964 (e) finite elements.

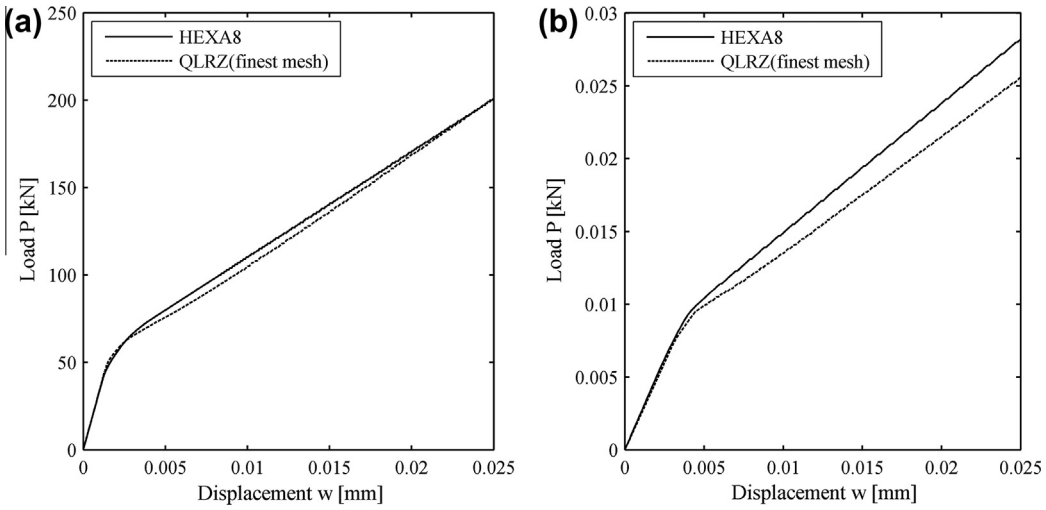

Fig. 7. Load vs vertical displacement for laminate **L1** (a) and **L2** (b).

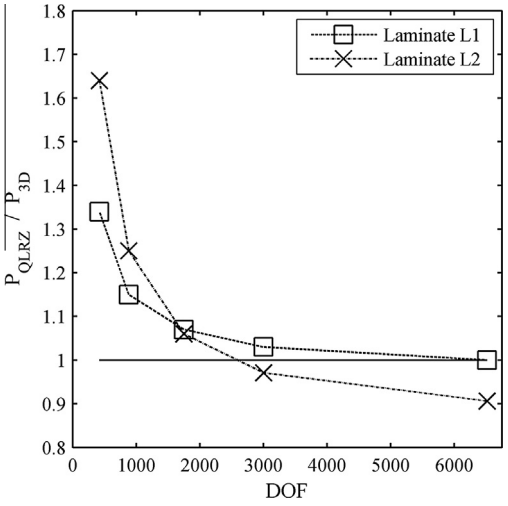

Fig. 8. Mesh convergence. Normalized load value for both laminates and all meshes.

$$\mathbf{a}^{(e)} = \sum_{i=1}^{4} \mathbf{N}_i \mathbf{a}_i^{(e)} \tag{11}$$

with

$$\mathbf{N}_i = N_i \mathbf{I}_7 \quad \text{and} \quad \mathbf{a}_i^{(e)} = \begin{bmatrix} u_0 & v_0 & w_0 & \theta_x & \theta_y & \psi_x & \psi_y \end{bmatrix}_i^T$$

being N_i the linear C^0 continuous shape function of node ith.

The generalized strains $\hat{\boldsymbol{\varepsilon}}$ of Eq. (4) are expressed in term of the nodal degrees of freedom (DOF) using Eq. (11) as

$$\hat{\boldsymbol{\varepsilon}} = \sum_{i=1}^{4} \mathbf{B}_i \cdot \mathbf{a}_i^{(e)} = \mathbf{B} \cdot \mathbf{a}^{(e)} \tag{12}$$

being $\mathbf{B}_i$ the generalized strain matrix defined as

$$\mathbf{B}_i = \begin{bmatrix} \mathbf{B1} \\ \mathbf{B2} \\ \mathbf{B3} \\ \mathbf{B4} \end{bmatrix}_i \tag{13}$$

with

$$\mathbf{B1}_i = \begin{bmatrix} \frac{\partial N_i}{\partial x} & 0 & 0 & 0 & 0 & 0 & 0 \\ 0 & \frac{\partial N_i}{\partial y} & 0 & 0 & 0 & 0 & 0 \\ \frac{\partial N_i}{\partial y} & \frac{\partial N_i}{\partial x} & 0 & 0 & 0 & 0 & 0 \end{bmatrix} \quad \mathbf{B2}_i = \begin{bmatrix} 0 & 0 & 0 & \frac{\partial N_i}{\partial x} & 0 & 0 & 0 \\ 0 & 0 & 0 & 0 & \frac{\partial N_i}{\partial y} & 0 & 0 \\ 0 & 0 & 0 & \frac{\partial N_i}{\partial y} & \frac{\partial N_i}{\partial x} & 0 & 0 \end{bmatrix}$$

$$\mathbf{B3}_i = \begin{bmatrix} 0 & 0 & 0 & 0 & 0 & \frac{\partial N_i}{\partial x} & 0 \\ 0 & 0 & 0 & 0 & 0 & 0 & \frac{\partial N_i}{\partial y} \\ 0 & 0 & 0 & 0 & 0 & \frac{\partial N_i}{\partial y} & 0 \\ 0 & 0 & 0 & 0 & 0 & 0 & \frac{\partial N_i}{\partial x} \end{bmatrix} \quad \mathbf{B3}_i = \begin{bmatrix} 0 & 0 & \frac{\partial N_i}{\partial x} & -N_i & 0 & 0 & 0 \\ 0 & 0 & \frac{\partial N_i}{\partial y} & 0 & -N_i & 0 & 0 \\ 0 & 0 & 0 & 0 & 0 & N_i & 0 \\ 0 & 0 & 0 & 0 & 0 & 0 & N_i \end{bmatrix} \tag{14}$$

The element stiffness matrix $\mathbf{K}^e$ and the external forces are obtained by using the virtual work principle and Eqs. (8), (10) and (12)

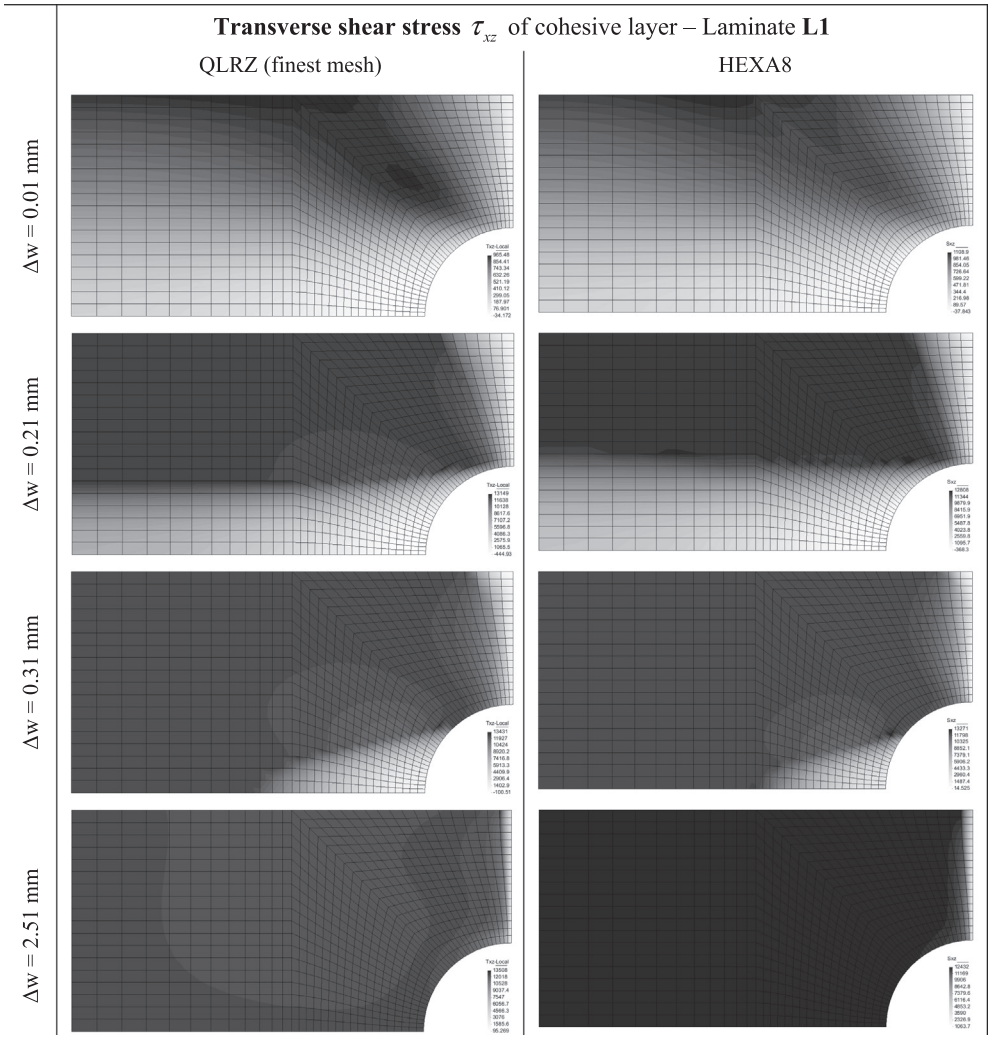

Fig. 9. Transverse shear distribution τ_{xz} of cohesive layer for laminate **L1** computed by using the finest QLRZ mesh (left) and the HEXA8 mesh (right) observed at four different Δw increments.

$$\mathbf{K}^e = \iint_A \mathbf{B}^T \widehat{\mathbf{D}} \mathbf{B}\, dA; \quad \mathbf{F}^e = \iint_A \mathbf{q}\, dA + \sum_{i=1}^{npl} \mathbf{f}_i \tag{15}$$

where A is the in-plane area of the finite element, q is the distributive load, f is the nodal force and $\widehat{\mathbf{D}}$ is the constitutive generalized matrix defined as

$$\widehat{\mathbf{D}} = \int_z [\mathbf{S}^k]^T \mathbf{D}^k \mathbf{S}^k\, dz \tag{16}$$

Full integration of matrix $\mathbf{K}^e$ by Gauss quadrature leads to shear locking for slender plates. In order to avoid this defect an *assumed transverse shear strain field*..[25] is used. Details of the formulation of the 4-noded QLRZ plate finite element can be found in [1,25].

3. Isotropic damage model

The non-linear behavior of material is managed by an isotropic damage model [2]. The level of damage is measured by a single internal scalar variable d, which takes values ranged between 0 (no damage) and 1 (full damage). The relationship between stresses and strains is written as

$$\boldsymbol{\sigma} = (1-d)\boldsymbol{\sigma}_0 = (1-d)\mathbf{D}_0 \cdot \boldsymbol{\varepsilon} \tag{17}$$

being $\boldsymbol{\sigma}$, $\boldsymbol{\varepsilon}$ and $\mathbf{D}_0$ the stress, the strain and the undamaged constitutive tensors, respectively.

The damage criterion, which is used to distinguish between a damage state and an undamaged one, is defined as

$$F(\boldsymbol{\sigma}_0, d) = f(\boldsymbol{\sigma}_0) - c(d) \leqslant 0 \tag{18}$$

where $f(\boldsymbol{\sigma}_0)$ is a norm used to compare different states of deformation and $c(d)$ is the damage threshold. Damage occurs when the value of $f(\boldsymbol{\sigma}_0)$ is larger than $c(d)$. Damage starts for $f(\boldsymbol{\sigma}_0) > c_0$, being c_0 the initial damage threshold value which depends on the material properties.

In this work, c_0 is defined as

$$c_0 = \frac{f_t}{\sqrt{E_0}} \tag{19}$$

where f_t is the tensile strength and E_0 the Young modulus of the undamaged material.

The proposed norm is

$$f(\boldsymbol{\sigma}_0) = \sqrt{\boldsymbol{\varepsilon} : \boldsymbol{\sigma}_0} \tag{20}$$

The evolution law for the damage threshold and the damage variable d are obtained using the damage consistency parameter according to the Kuhn–Tucker conditions. The evolution of these variables can be explicitly integrated [33] to obtain

$$\begin{aligned} d &= \Omega(f(\boldsymbol{\sigma}_0)) \\ c(d) &= \max\{c_0; \max\{f(\boldsymbol{\sigma}_0)\}\} \end{aligned} \tag{21}$$

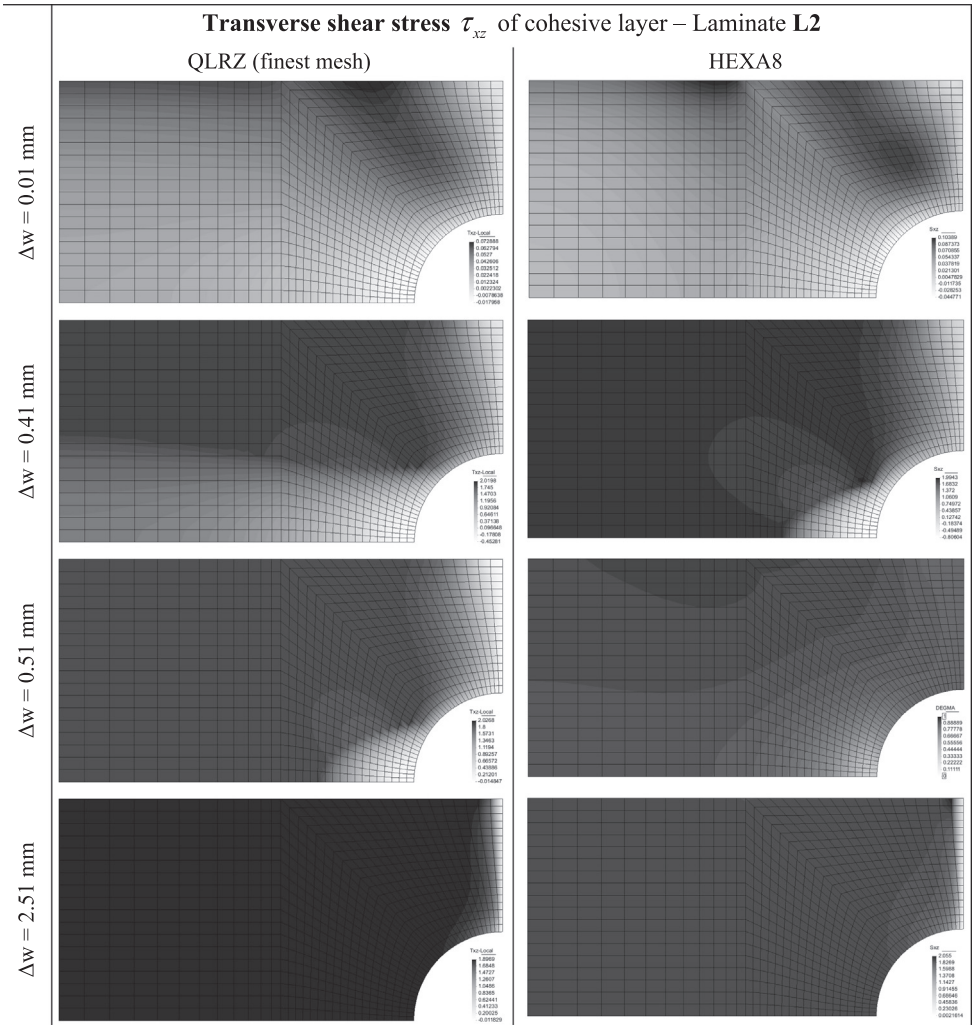

Fig. 10. Transverse shear distribution τ_{xz} of cohesive layer for laminate **L2** computed by using the finest QLRZ mesh (left) and the HEXA8 mesh (right) observed at four different Δw increments.

where $\Omega(\bullet)$ is a monotonic scalar function ranging between 0 and 1 which defines the evolution of the damage variable. In this work, an exponential evolution law is adopted for Ω as

$$\Omega(f(\boldsymbol{\sigma}_0)) = 1 - \frac{f^0(\boldsymbol{\sigma}_0)}{f(\boldsymbol{\sigma}_0)} e^{B\left(1-\frac{f(\boldsymbol{\sigma}_0)}{f^0(\boldsymbol{\sigma}_0)}\right)} \quad \text{with} \quad f^0(\boldsymbol{\sigma}_0) = c_0 \tag{22}$$

Considering the norm of Eq. (20), the exponential softening function of Eq. (22), and the initial damage threshold value c_0 (Eq. (19)), the parameter B in Eq. (22) is computed as

$$B = \left(\frac{G_f \cdot E_0}{l^* \cdot (f_t)^2} - \frac{1}{2}\right)^{-1} \geqslant 0 \tag{23}$$

being G_f the fracture energy per unit area and l^* a characteristic length. In this paper, l^* is defined as the square root of the influence area of each Gauss point.

Finally, the evolution equation of the variable d is written as

$$d = 1 - \frac{c_0}{\sqrt{\boldsymbol{\varepsilon} : \boldsymbol{\sigma}_0}} e^{B\left(1-\frac{\sqrt{\boldsymbol{\varepsilon}:\boldsymbol{\sigma}_0}}{c_0}\right)} \tag{24}$$

4. Update of the zigzag function ϕ to simulate delamination

During a material degradation process, the structure stiffness suffers changes that induce a non-linear response of the structure. The resulting non-linear set of equilibrium equations can be schematically written as

$$\mathbf{F}^{\text{ext}} - \mathbf{F}^{\text{int}}(\mathbf{q}) = \mathbf{R}(\mathbf{q}) \tag{25}$$

where $\mathbf{q}$, $\mathbf{F}^{\text{ext}}$ and $\mathbf{F}^{\text{int}}$ $(\mathbf{q})$ are the discretization parameters, the external and the internal forces vectors, respectively. $\mathbf{R}(\mathbf{q})$ is the residual forces vector. In this work, dynamic forces are not considered.

The non-linear equation system of Eq. (25) is solved whit a modified Newton–Raphson method. Hence, the following linear problem is solved for each iteration i

$$d\mathbf{q} = ({}^{i-1}\mathbf{K}_{\text{d}})^{-1}\, {}^{i-1}\mathbf{R} \tag{26}$$

where $d\mathbf{q}$ is the increment of the nodal DOF at ith iteration. $\mathbf{K}_{\text{d}}$ and $\mathbf{R}$ are the damaged stiffness matrix and the residual vector, respectively, which are computed at the previous $i-1$th iteration. For the QLRZ element matrix $\mathbf{K}_{\text{d}}$ is defined as

$${}^{i-1}K_d = \iint_A \mathbf{B}^T\, {}^{i-1}\widehat{\mathbf{D}}_d \mathbf{B}\, dA \tag{27}$$

with

$${}^{i-1}\widehat{\mathbf{D}}_{\text{d}} = \int_z \left[{}^{i-1}\mathbf{S}^k\right]^T {}^{i-1}\mathbf{D}_{\text{d}}^k\, {}^{i-1}\mathbf{S}^k\, dz \quad \text{and} \quad {}^{i-1}\mathbf{D}_{\text{d}}^k = (1 - {}^{i-1}d^k)\, \mathbf{D}_0^k \tag{28}$$

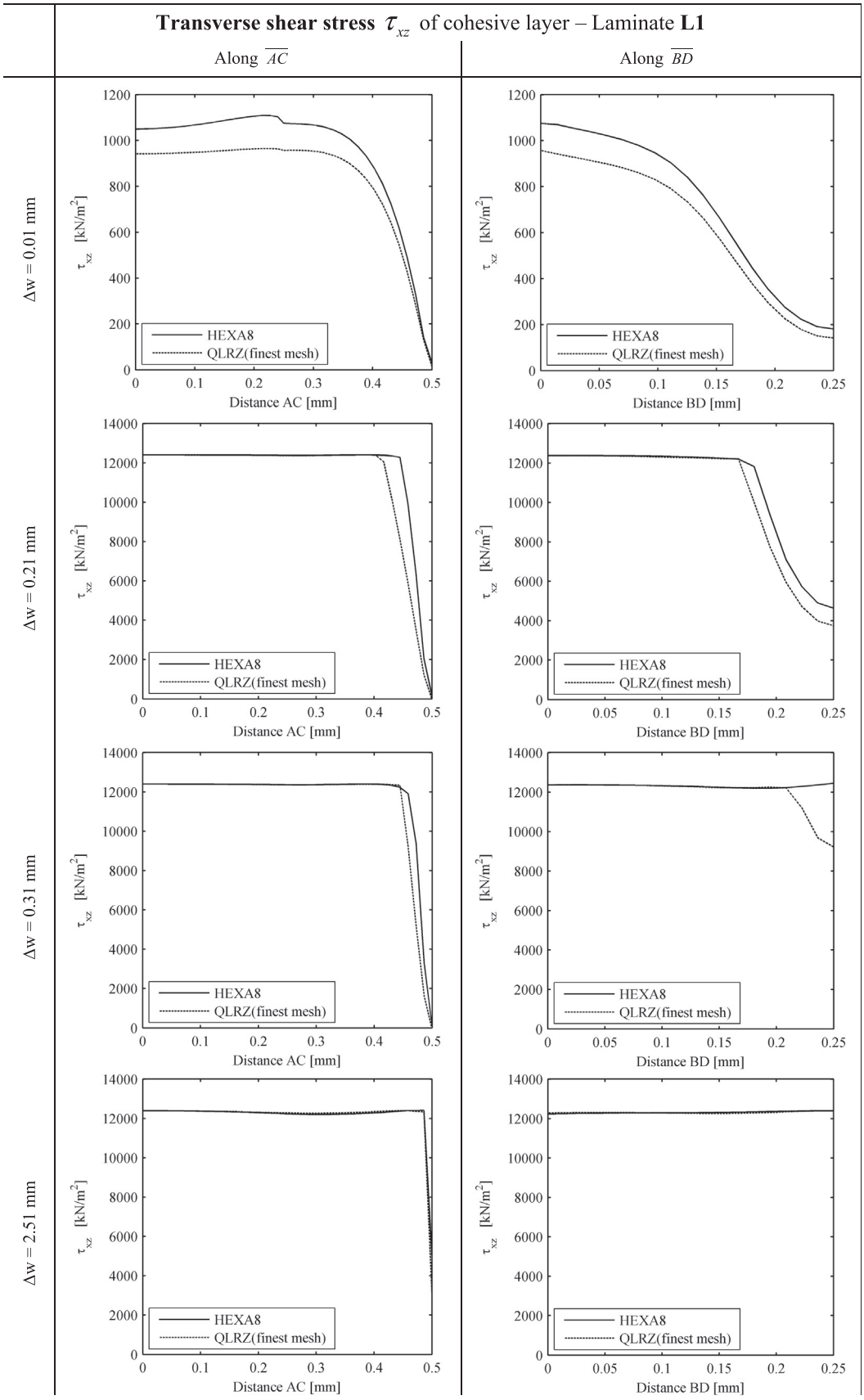

Fig. 11. Transverse shear distribution τ_{xz} of cohesive layer for laminate **L1** along the segments $\overline{AC}$ (left) and $\overline{BD}$ (right), which were observed at four different Δw increments.

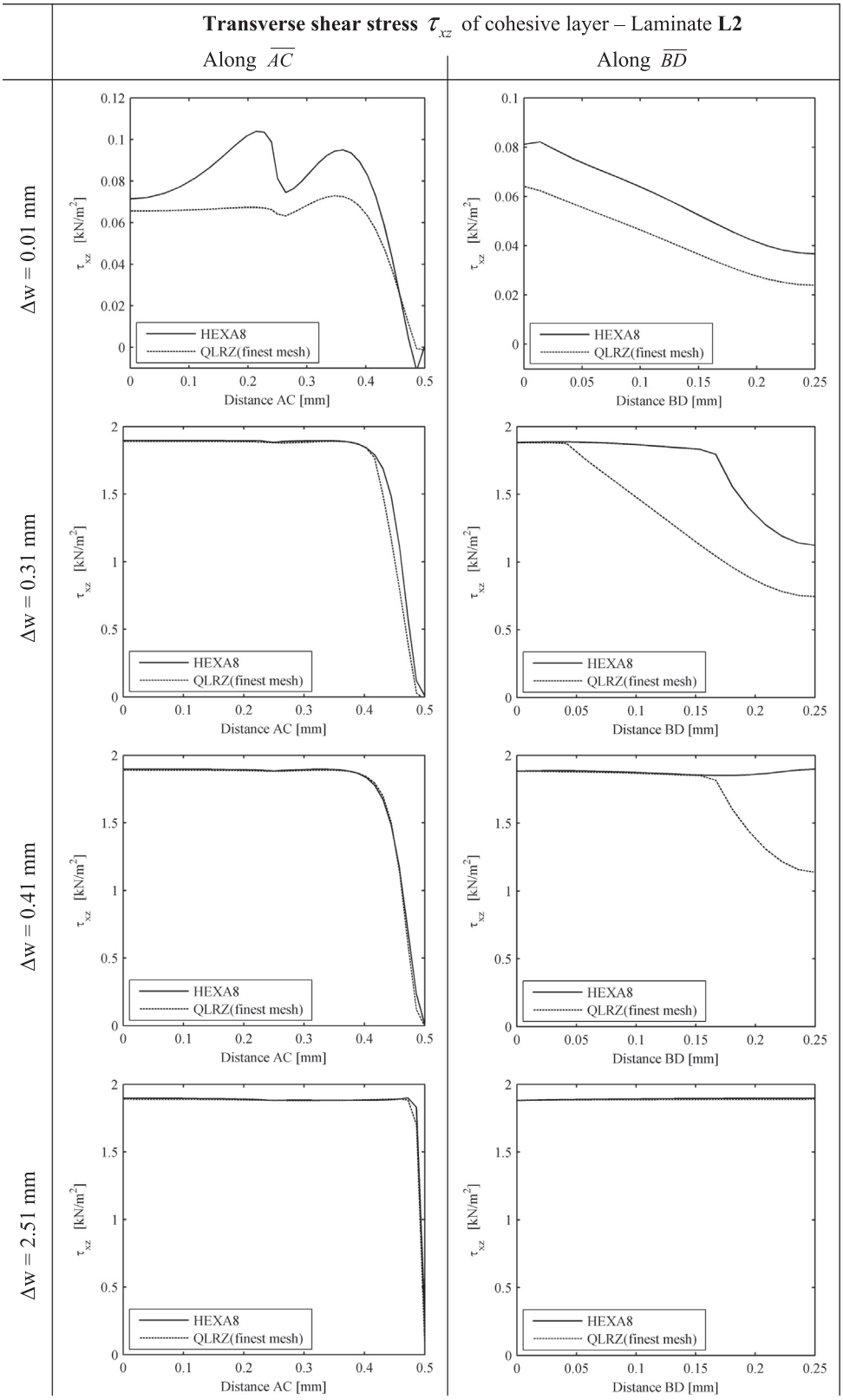

Fig. 12. Transverse shear distribution τ_{xz} of cohesive layer for laminate **L2** along the segments $\overline{AC}$ (left) and $\overline{BD}$ (right), which were observed at four different Δw increments.

where d^k is the scalar damage variable for the kth computed by equation Eq. (24) at the previous $i-1$th iteration.

The nodal DOFs are updated by

$$^{i}\mathbf{q} = {}^{i-1}\mathbf{q} + d\mathbf{q} \tag{29}$$

The process is repeated until the convergence criterion $\|\mathbf{R}\| \leqslant \varsigma\|\mathbf{F}^{ext}\|$ is satisfied where ς is a predefined error tolerance [34].

In 3D finite element analysis, the nodal internal forces are obtained by integrating the stresses on the finite element volume. When any finite element exceeds the damage threshold and suffers

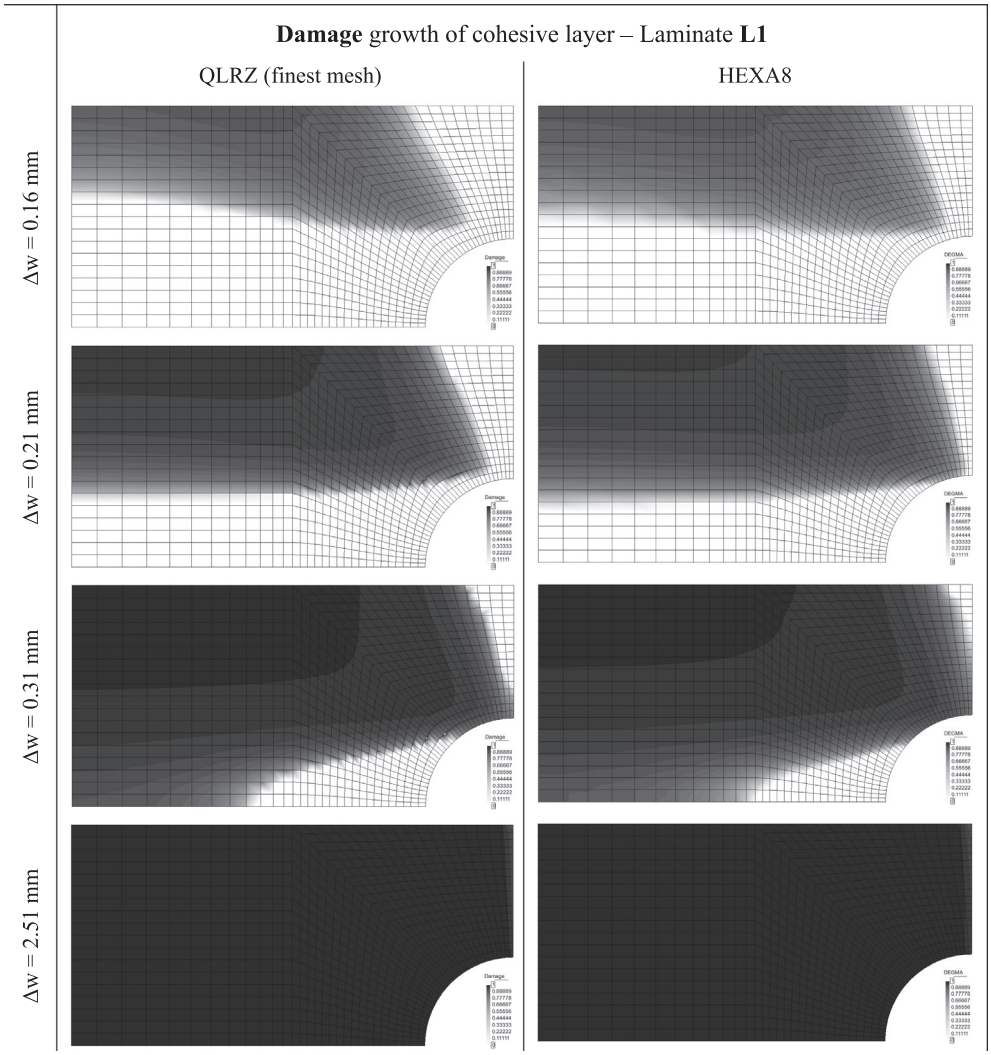

Fig. 13. Damage level of cohesive layer for laminate **L1** computed by using the finest QLRZ mesh (left) and the HEXA8 mesh (right) observed at four different Δw increments. White color is a sing of non-damage and black color indicates full damage.

softening ($d > 0$), its stresses are reduced by Eq. (17). Thus, a lack of internal force equilibrium between the damaged element and its neighbors appears which induces residual forces (**R**). These residual forces generate the relative displacement between layers that typically occurs during a delamination process. Equilibrium is achieved using an iterative process such as that of Eqs. (26) and (29).

For the QLRZ finite element, the kinematic variables (Eq. (2)) and the stress resultants (Eq. (10)) are computed at the in-plane middle surface of the plate ($z = 0$). Because of that, unlike the 3D analysis, there are no forces within the laminate capable of inducing a relative displacement between plies. Thus, it is not possible to predict delamination with QLRZ element by only reducing the stresses using Eq. (17). Therefore, if the stresses are reduced only, the iterative process (Eqs. (26) and (29)) gives as result an amplification of the initial kinematics of the laminate, instead of an update of the delaminated kinematics. That is so, because the variables of Eq. (2) are not capable to modify by themselves the zigzag form of the axial displacement, but they can only vary the scale of the original zigzag distribution.

The kinematics of the RZT theory is defined by a superposition of a linear piecewise zigzag function over the linear FSDT displacement fields (Fig. 1). As a result, the zigzag shape of the laminate kinematics is governed by only the zigzag function ϕ. Comprehensibly, in order for capturing the relative displacement using the QLRZ element, it is indispensable to update the zigzag function. In this work, the update of ϕ is expressed as a function of the damage variable d. The zigzag function ϕ depends on the shear modulus, thus, it is updated by reducing the initial elastic shear modulus G^k_{iz} at the damaged kth layer as

$$\widetilde{G}^k_{iz} = (1 - d^k) G^k_{iz} \tag{30}$$

which leads to the definition of ϕ in term of the damaged shear modulus as

$$\phi^k_i = \bar{\phi}^{k-1}_i + \frac{h^k \tilde{\beta}^k_i}{2}(\zeta^k + 1) \tag{31}$$

with

$$\tilde{\beta}^k_i = \frac{\widetilde{G}_{iz}}{\widetilde{G}^k_{iz}} - 1 \quad \text{and} \quad \widetilde{G}_{iz} = h\left[\sum_{k=1}^{N} \frac{h^k}{\widetilde{G}^k_{iz}}\right]^{-1} \tag{32}$$

This simple update procedure of the zigzag function ϕ allows us to capture the relative displacement in a delamination process. All above-mentioned steps are schematized in Fig. 2.

The algorithm to solve the non-linear equilibrium problem of Eq. (25) is shown in Fig. 3.

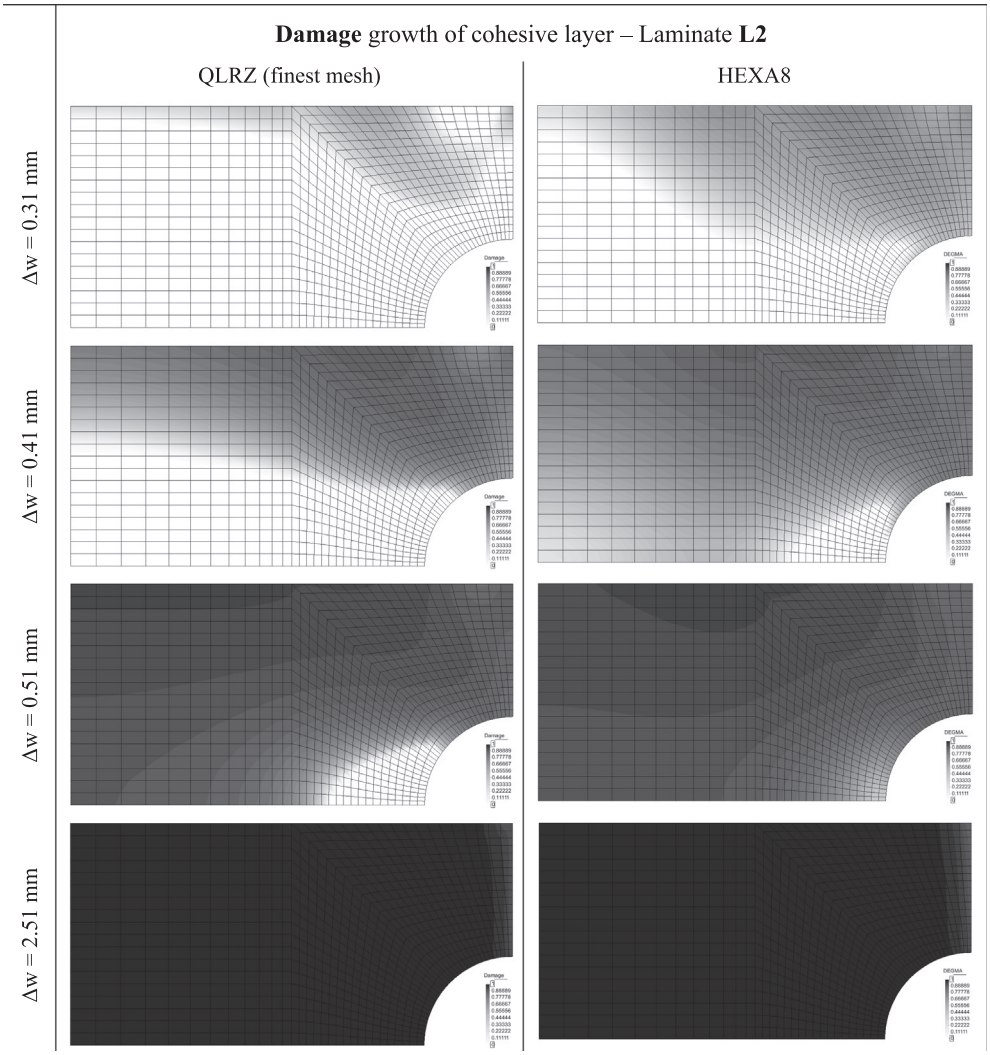

Fig. 14. Damage level of cohesive layer for laminate **L2** computed by using the finest QLRZ mesh (left) and the HEXA8 mesh (right) observed at four different Δw increments. White color is a sing of non-damage and black color indicates full damage.

5. Numerical simulations

The capability of the proposed method for capturing the relative in-plane displacements (Mode II and III) between plies is studied by modeling a simply supported rectangular plate of length $L = 1.0$ m, depth $D = 0.5$ m and thickness $h = 0.025$ m with a center hole of radius $R = 0.0125$ m (Fig. 4a). Taking advantage of symmetry, only one quarter of plate is studied (Fig. 4b). The structure is subjected to bending by imposing a uniform vertical displacement Δw along the line $\overline{CF}$ (Fig. 4b). The plate is analyzed for two laminates (L1 and L2) with properties shown in Tables 1–3.

As any laminate ply is capable to suffer damage, it is not necessary to predefine the delamination path. However, in order to show the capability of the QLRZ element to capture relative displacement between plies, in this work delamination is forced to take place at only one predefined interface within each laminate. This interface is modeled by a ply, called "cohesive layer" (cl) henceforth, whose mechanical behavior is modeled by the isotropic damage model of Section 3. Thus, delamination occurs when the cohesive layer starts to be damaged. The other plies are treated as linear-elastic.

The analysis was carried out under the following considerations: quasi-static application of vertical displacement, geometrically linear conditions and small deformations.

The reference solution was obtained via a 3D finite element analysis using a mesh of 16,416 8-noded hexahedral elements (HEXA8) involving 18,620 nodes and 55,860 DOFs (Fig. 5). One and two finite elements are used to discretize the thickness of the cohesive layer and the thickness of the elastic layers, respectively. This mesh was used for both laminates as they share the same geometry.

Mesh convergence is studied using five QLRZ meshes of 44, 102, 216, 384 and 964 finite elements with 60, 126, 250, 429, 931 nodes and 420, 882, 1750, 3003, 6517 DOF, respectively, as shown in Fig. 6.

The load–displacement plot for laminates L1 and L2 is shown in Figs. 7a and 6b, respectively. The curves are obtained with the HEXA8 element (solid line) and the finest QLRZ mesh (dashed lines). The load corresponds to the total vertical reaction computed at the simply supported end and an imposed vertical displacement Δw (Fig. 4b). Results show a good agreement between both solution techniques. In all cases, the lineal-elastic QLRZ stiffness is very close to that computed using 3D analysis. Also, it is shown that delamination starts approximately at the same values of displacement and load.

Fig. 8 shows the convergence of the normalized load value at the end of the simulation as the number of DOF is increased. The error for the coarser QLRZ mesh reaches almost 35% and 65% for

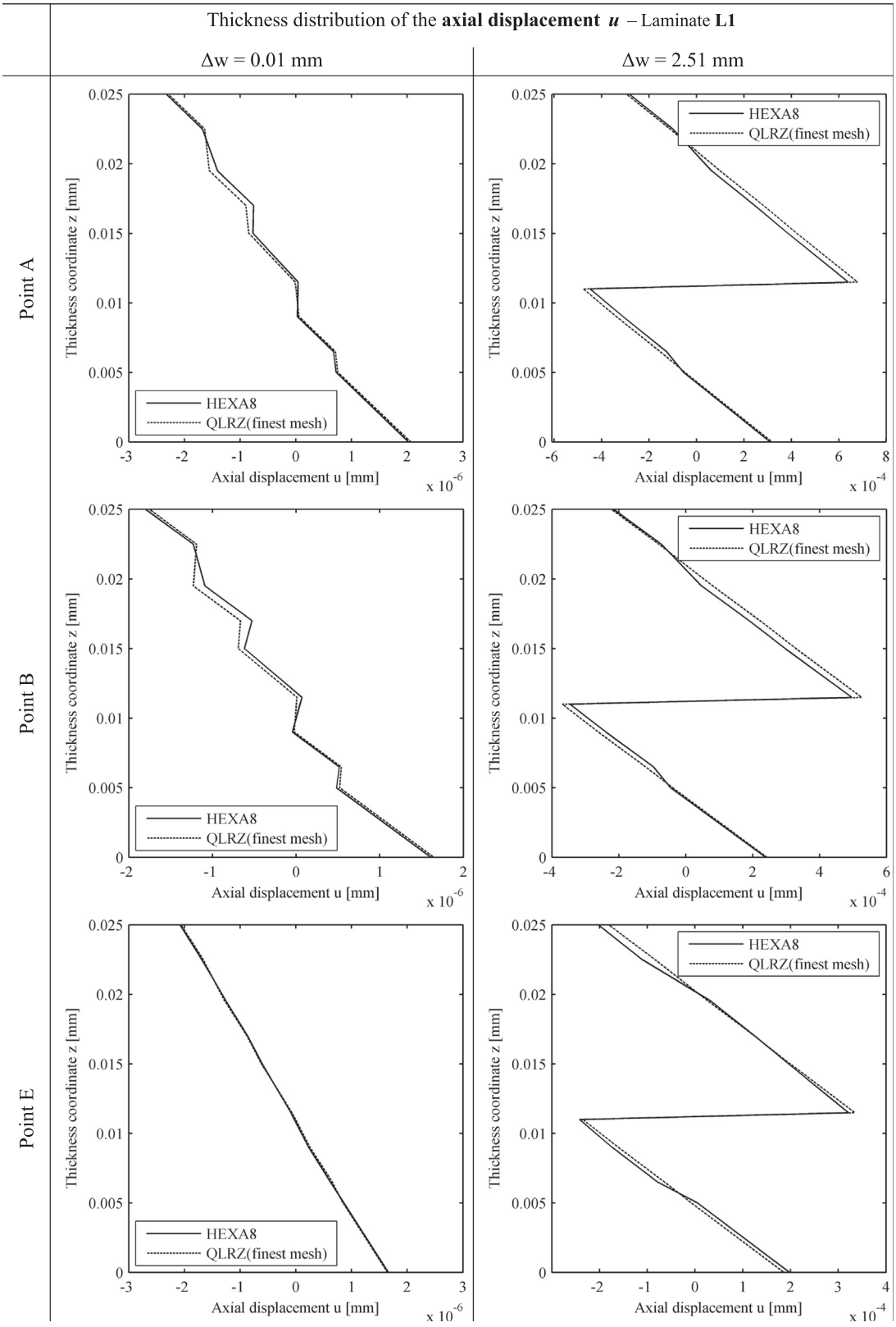

Fig. 15. Thickness distribution of the axial displacement u at three different points for laminate **L1**. Figures show the undamaged kinematics (left – $\Delta w = 0.01$ mm) and the delaminated kinematics at the end of simulation (right – $\Delta w = 2.51$ mm).

laminates L1 and L2, respectively. However, the error is around 1% (L1) and 10% (L2) for the finest QLRZ mesh.

The evolution of the transverse shear stress τ_{xz} for the cohesive layer for laminates L1 and L2 is shown in Figs. 9 and 10, respectively. For the linear-elastic state, the HEXA8 solution gives about 12% (L1) and 30% (L2) higher maximum value of τ_{xz} as appreciated for $\Delta w = 0.01$ mm. Because of that, damage starts a little later for the QLRZ solution. This mismatch between both solutions is more

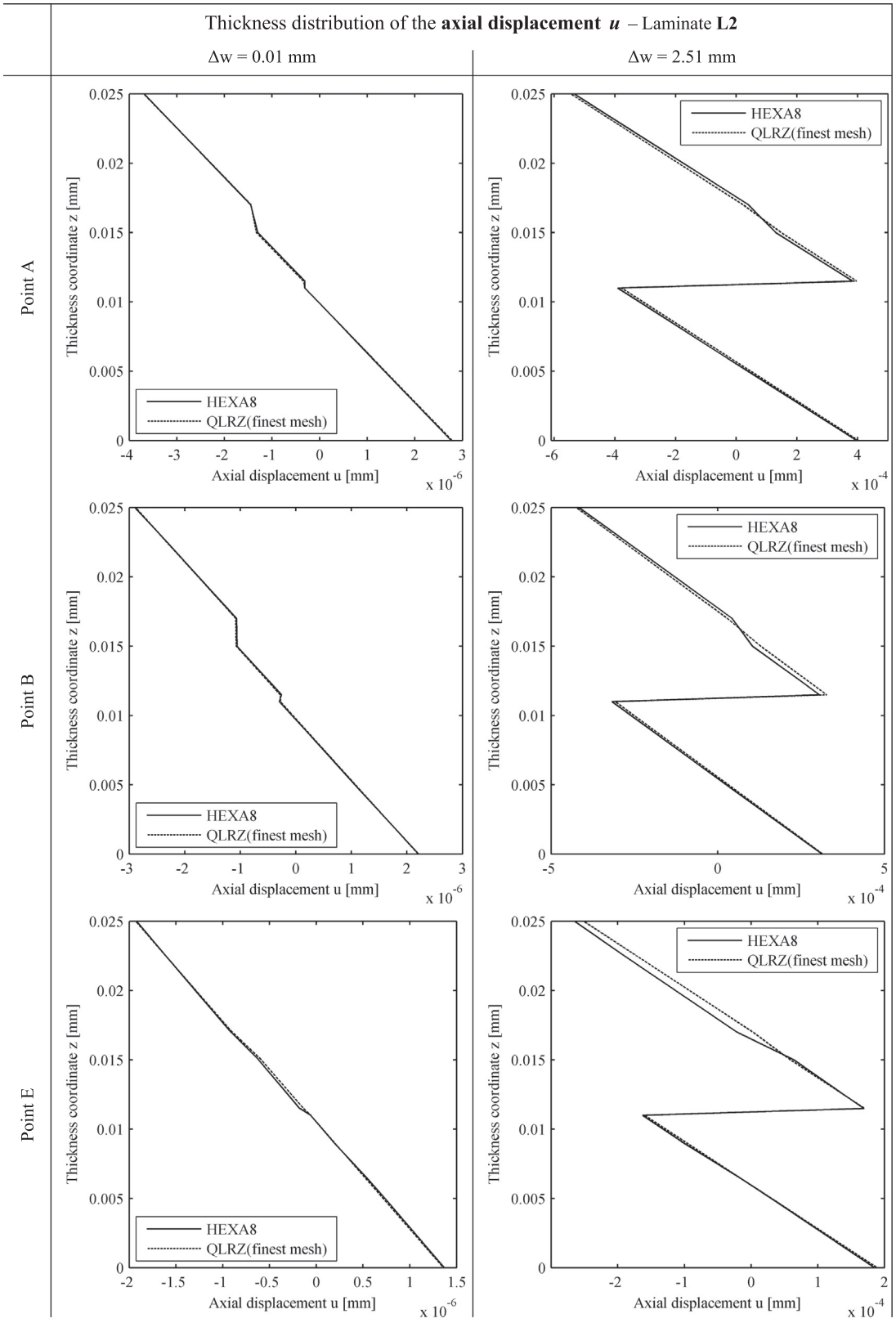

Fig. 16. Thickness distribution of the axial displacement u at three different points for laminate **L2**. Figures show the undamaged kinematics (left – $\Delta w = 0.01$ mm) and the delaminated kinematics at the end of simulation (right – $\Delta w = 2.51$ mm).

evident for the L2 laminate where the τ_{xz} distribution obtained with the HEXA8 mesh for $\Delta w = 0.41$ mm is similar to that computed using the QLRZ mesh for $\Delta w = 0.51$ mm. For the L1 laminate, no great differences are observed between both solutions. In all cases, approximately the same values of τ_{xz} are predicted at the end of the simulation ($\Delta w = 2.51$ mm). In order to clarify theses situations the distribution of τ_{xz} along segments $\overline{AC}$ and $\overline{BD}$ (Fig. 4b) for different increment steps is presented in Figs. 11(L1) and 12

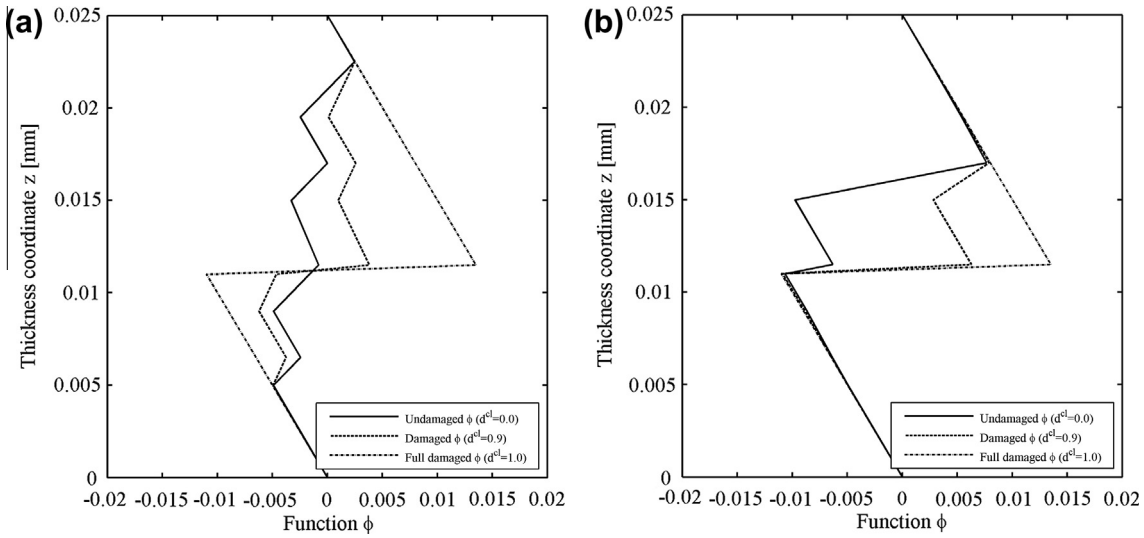

Fig. 17. Undamaged and damaged zigzag function ϕ_x for laminate L1 (a) and L2 (b).

(L2). Results are influenced by the mesh topology specially for laminate L2 as is shown in Fig. 12 for $\Delta w = 0.01$ mm. However, this mesh dependence disappears once delamination has started.

The greyscale images shown in Figs. 13 and 14 illustrate the damage growth of the cohesive ply for laminates L1 and L2, respectively. The black color denotes a full damage state ($d = 1$). These images confirm that damage starts earlier when the HEXA8 finite elements are used, especially for the L2 laminate. However, the global response of the structure (Fig. 7) is similar for both finite elements.

Although the cohesive layer seems to be full damaged at the last step ($\Delta w = 2.51$ mm), the damage variable just reaches at most a value of 0.997. For this reason, the transverse shear stress τ_{xz} did not decrease as expected in a softening process. Surely, if the test continues until the ply is full damaged, the stresses will be reduced to zero.

The thickness distribution of the axial displacement u at points A, B and E (Fig. 4b), before ($\Delta w = 0.01$ mm) and after ($\Delta w = 2.51$ mm) delamination, is plotted in Figs. 15 (L1) and 16 (L2), respectively. The QLRZ element captures the relative displacement with errors less than 6% and 2% for laminates L1 and L2, respectively. For all cases, a very good match between 3D and QLRZ kinematics was found.

To emphasize the importance of the zigzag function update to capture relative displacement between layers during a delamination process, Fig. 17 shows the change of the zigzag thickness distribution from an undamaged to a full damaged state for laminates L1 (Fig. 17a) and L2 (Fig. 17b).

In order to compare the performance of the 3D solution and the QLRZ analysis, both the total increment numbers and incremental displacement values as well as the error tolerance value are the same for both methods. As expected, the computation time needed for the QLRZ solution is several times less than that required for the 3D analysis. The time used by the finest QLRZ mesh is approximately 20 and 12 times less than that required by the HEXA8 mesh for laminates L1 and L2, respectively. In addition, the computation storage space during the simulation is much greater for the 3D analysis as expected.

6. Conclusions

We have presented a promising numerical method based on the refined zigzag theory for modeling delamination in laminated plate/shell structures. The proposed method uses the quadrilateral QLRZ finite element for predicting the laminate kinematics and an isotropic damage model for managing the non-linear material behavior. The proposed formulation can model the fracture modes II and III. However, this methodology is unable to simulate the fracture mode I as the vertical displacement is constant through the laminate thickness. In addition, the use of this technique is limited to laminates where the shear modulus of the laminae does not differ from each other in many orders of magnitude, which occurs generally in laminated composite materials.

We have shown the need of updating the zigzag function so that it can capture the relative displacement between plies. The proposed update depends on the level of degradation. Therefore, both the stresses and the zigzag function are influenced by the damage variable during the iterative process.

The performance of the QLRZ element has been studied by simulating delamination in a simply supported rectangular plate with a center hole subjected to bending. The reference solution was obtained whit a 3D finite element analysis. Results show that both the onset and the evolution of delamination are accurately predicted by the QLRZ element. Also, the delaminated kinematics at the end of simulation is well predicted whit the new plate element.

Acknowledgements

The first author acknowledges the FPU-UPC scholarship from the Universitat Politècnica de Catalunya and the Ministerio de Educación of Spain.

This research was partially financial supported by the SAFECON project of the European Research Council (ERC) of the European Commission.

References

[1] Eijo A, Oñate E, Oller S. A four-noded quadrilateral element for composite laminated plates/shells using the refined zigzag theory. Int J Numer Methods Eng 2013. <http://dx.doi.org/10.1002/nme.4503>.

[2] Oliver J, Cervera M, Oller S, Lubliner J. Isotropic damage models and smeared crack analysis of concret. In: Second international conference on computer aided analysis and design of concrete structures. Zell am See, Austria; 1990.

[3] Bolotin VV. Delaminations in composite structures: its origin, buckling, growth and stability. Composites: Part B 1996;27B:129–45.

[4] Krueger R. The virtual crack closure technique: history, approach and applications. Appl Mech Rev 2002;57(2):109–43.

[5] Mabson G. Fracture analysis for bondlines and interfaces of composite structures. In: 4th international conference on composites testing and model identification (Comptest2008), Dayton (OH); October 2008.

[6] Liu PF, Hou SJ, Chu JK, Hu XY, Zhou CL, Liu YL, et al. Finite element analysis of postbuckling and delamination of composite laminates using virtual crack closure technique. Compos Struct 2011;93(6):1549–60.

[7] Balzani C, Wagner W. An interface element for the simulation of delamination in unidirectional fiber-reinforced composite laminates. Eng Fract Mech 2008;75(9):2597–615.
[8] Wagner W, Balzani C. Simulation of delamination in stringer stiffened fiber-reinforced composite shells. Comput Struct 2008;86(9):930–9.
[9] Turon A, Camanho PP, Costa J, Renart J. Accurate simulation of delamination growth under mixed-mode loading using cohesive elements: definition of interlaminar strengths and elastic stiffness. Compos Struct 2010;92(8):1857–64.
[10] Borg R, Nilsson L, Simonsson K. Modeling of delamination using a discretized cohesive zone and damage formulation. Compos Sci Technol 2002;62(10–11):1299–314.
[11] Liu PF, Islam MM. A nonlinear cohesive model for mixed-mode delamination of composite laminates. Compos Struct 2013;106:47–56.
[12] Martinez X, Rastellini F, Oller S, Flores F, Oñate E. Computationally optimized formulation for the simulation of composite materials and delamination failures. Composites: Part B 2011;47:134–44.
[13] Reissner E. The effect of transverse shear deformation on the bending of elastic plates. Appl Mech 1945;12:69–79.
[14] Mindlin RD. Influence of rotatory inertia and shear in flexural motions of isotropic elastic plates. Appl Mech 1951;18:1–38.
[15] Reddy JN, Robbins DH. Theories and computational models for composite laminates. Appl Mech Rev 1994;47(6):147–69.
[16] Reddy JN. A generalization of two-dimensional theories of laminated plates. Commun Appl Numer Methods 1987;3(3):173–80.
[17] Liu D, Li X. An overall view of laminate theories based on displacement hypothesis. J Compos Mater 1996;30(14):1539–61.
[18] Carrera E. Mixed layer-wise models for multilayered plates analysis. Compos Struct 1998;43(1):57–70.
[19] Wanji C, Zhen W. A selective review on recent development of displacement-based laminated plate theories. Recent Patents Mech Eng 2008;1:29–44.
[20] Carrera E. Historical review of zig–zag theories for multilayered plates and shells. Appl Mech Rev 2003;56(3):287–308.
[21] Kumar A, Chakrabarti A, Bhargava P. Finite element analysis of laminated composite and sandwich shells using higher order zigzag theory. Compos Struct 2013;106:270–81.
[22] Tessler A, Sciuva MD, Gherlone M. Refined zigzag theory for homogeneous, laminated composite, and sandwich plates: a homogeneous limit methodology for zigzag function selection. Numer Methods Part Diff Eq 2011;27(1):208–29.
[23] Tessler A, Sciuva MD, Gherlone M. A consistent refinement of first-order shear deformation theory for laminated composite and sandwich plates using improved zigzag kinematics. Mech Mater Struct 2010;5(2):341–65.
[24] Tessler A, Sciuva MD, Gherlone M. A refined zigzag beam theory for composite and sandwich beams. J Compos Mater 2009;43(9):1051–81.
[25] Oñate E. Structural analysis by the finite element method. Beams, plates and shells, vol. 2. Barcelona: Springer-CIMNE; 2013.
[26] Gherlone M, Tessler A, Di Sciuva M. C^0 beam element based on the refined zigzag theory for multilayered composite and sandwich laminates. Compos Struct 2011;93:2882–94.
[27] Oñate E, Eijo A, Oller S. Simple and accurate two-noded beam element for composite laminated beams using a refined zigzag theory. Comput Methods Appl Mech Eng 2012:362–82.
[28] Barbero EJ, Reddy JN. Modeling of delamination in laminates using a layer-wise plate theory. Int J Solids Struct 1991;28(3):373–88.
[29] Na WJ, Reddy JN. Delamination in cross-ply laminated beams using the layerwise theory. Asian J Civ Eng 2009;10:451–80.
[30] Icardi U, Zardo G. C0 Plate element for delamination damage analysis, based on a zig–zag model and strain energy updating. Int J Impact Eng 2005;31(5):579–606.
[31] Eijo A, Oñate E, Oller S. A numerical model of delamination in composite laminated beams using the LRZ beam element based on the refined zigzag theory. Compos Struct 2013:270–80. http://dx.doi.org/10.1016/j.compstruct.2013.04.035.
[32] Soden PD, Hinton MJ, Kaddour AS. Lamina properties, lay-up configurations and loading conditions for a range of fibre-reinforced composite laminates. Compos Sci Technol 1998;58:1011–22.
[33] Oller S. Fractura mecánica. Un enfoque global. Barcelona, España: CIMNE; 2001. ISBN: 84-89925-76-3.
[34] Zienkiewicz OC, Taylor RL. El método de los elementos finitos, 5th ed., vol. 2. Barcelona: CIMNE; 2004. ISBN: 84-95999-53-6.